Carbonic anhydrase XIV is enriched in specific membrane domains of retinal pigment epithelium, Müller cells, and astrocytes

Erlend A. Nagelhus*†‡, Thomas M. Mathiisen*, Allen C. Bateman*, Finn-M. Haug*, Ole P. Ottersen*, Jeffrey H. Grubb§, Abdul Waheed§, and William S. Sly‡§

*Nordic Centre for Water Imbalance Related Disorders and Centre for Molecular Biology and Neuroscience, Institute of Basic Medical Sciences, University of Oslo, P.O. Box 1105, Blindern, N-0317 Oslo, Norway; †Department of Neurology, Rikshospitalet, N-0027 Oslo, Norway; and §Edward A. Doisy Department of Biochemistry and Molecular Biology, Saint Louis University School of Medicine, St. Louis, MO 63104

Contributed by William S. Sly, April 12, 2005

Carbonic anhydrases (CAs) are ubiquitous enzymes important to many cell types throughout the body. They help determine levels of H^+ and HCO_3^- and thereby regulate intracellular and extracellular pH and volume. CA XIV, an extracellular membrane-bound CA, was recently shown to be present in brain and retina. Here, we analyze the subcellular distribution of CA XIV in retina by high-resolution immunogold cytochemistry and show that the distribution in retina (on glial cells but not neurons) is different from that reported for brain (on neurons but not glia). In addition, CA XIV is strongly expressed on retinal pigment epithelium (RPE). The specific membrane domains that express CA XIV were endfoot and nonendfoot membranes on Müller cells and astrocytes and apical and basolateral membranes of RPE. Gold particle density was highest on microvilli plasma membranes of RPE, where it was twice that of glial endfoot and Müller microvilli membranes and four times that of other glial membrane domains. Neither neurons nor capillary endothelial cells showed detectable labeling for CA XIV. This enrichment of CA XIV on specific membrane domains of glial cells and RPE suggests specialization for buffering pH and volume in retinal neurons and their surrounding extracellular spaces. We suggest that CA XIV is the target of CA inhibitors that enhance subretinal fluid absorption in macular edema. In addition, CA XIV may facilitate CO_2 removal from neural retina and modulate photoreceptor function.

immunogold cytochemistry | pH regulation | CO_2/bicarbonate transport | glial endfeet | cystoid macular edema

Carbonic anhydrases (CAs) catalyze the reversible hydration of carbon dioxide to form bicarbonate and protons. At least 12 enzymatically active isozymes have been identified that differ in their tissue distribution and subcellular localization. Membrane-bound CA activity figures prominently in the regulation of extracellular pH. In the CNS, such CAs affect neuronal activity, reflecting the pH sensitivity of many synaptic molecules, including transporters and receptors (1). Important examples are glutamate transporters, which carry protons along with glutamate and sodium ions (2), and NMDA receptors, which are endowed with a proton binding site (3). Extracellular membrane-bound CAs facilitate transport of a number of organic ions by making protons and bicarbonate available for the transport process. Thus, CA activity increases significantly the transmembrane flux of lactate/H^+ through monocarboxylate transporters (MCTs) (4) and is also coupled functionally to sodium-dependent bicarbonate transporters (5).

CA inhibitors are used clinically for conditions as diverse as epilepsy, intracranial hypertension, cystoid macular edema, and glaucoma (6). Several intracellular (II, V, and VII) and extracellular (IV and XIV) CA isoforms have been demonstrated in the brain and eye (7–15). Of the intracellular isoforms, CA V is expressed in neuronal and glial mitochondria (10), and CA II is highly expressed in oligodendrocytes and in Müller cells in retina (9, 15). Of the membrane-bound isoforms in brain, CA IV has been demonstrated on the luminal surface of cortical capillary endothelial cells (16, 17) and on neurons and glia in selected regions of brain (18), and CA XIV has been found on neurons and axons in brain tissue (11). Thus, the CA XIV isoform may also be of importance for regulation of neuronal excitability and transport processes in brain.

Here, we have investigated the subcellular expression of CA XIV in mouse retina. Ridderstrale *et al.* (16), using a histochemical stain for CA activity, observed a membrane-associated CA activity in the ciliary body, retinal pigment epithelium (RPE), and Müller cells of CA II-deficient mice. Newman (19) also provided physiological evidence for enrichment of extracellular CA activity at glial endfoot membranes. Because CA IV was the only membrane-associated CA known at the time, this activity was assumed to be CA IV. However, Hageman *et al.* (17) had reported that CA IV, although highly expressed on the surface of endothelial cells of the choriocapillaris, was absent in retina. This discrepancy was clarified when Linser *et al.* (14) reported that the newly discovered membrane isoform, CA XIV, was highly expressed in Müller cells and the RPE. More recently, they reported that the intense CA XIV immunostaining in Müller cells and the RPE was absent in the CA XIV knockout mouse (15).

Retina is possibly the part of the CNS that has been characterized most extensively in regard to transport processes that might be directly or indirectly coupled to CA XIV activity (20). Because of its high metabolic activity, the retina generates a large amount of CO_2 and lactate. Moreover, the direction of transport is better defined in the retina than in the more complex neuropil of the brain. For example, the flux of lactate has been shown to occur constitutively from the inner to the outer aspect of the retina (18). Other transport processes may shift polarity depending on the metabolic activity. Our data show that glial cells and the RPE not only express CA XIV, but contain specific membrane domains that are highly enriched in CA XIV. CA XIV in these domains may be coupled to transport processes that require protons or bicarbonate and likely plays a role in pH and volume homeostasis in the extracellular space.

Methods

Animals. Male C57BL mice ($n = 15$) weighing ≈30 g (Folkehelseinstituttet, Oslo) were used in this study. The animals were allowed ad libitum access to food and drinking water.

Abbreviations: CA, carbonic anhydrase; RPE, retinal pigment epithelium; MCT, monocarboxylate transporter.

‡To whom correspondence may be addressed. E-mail: e.a.nagelhus@medisin.uio.no or slyws@slu.edu.

www.pnas.org/cgi/doi/10.1073/pnas.0503021102

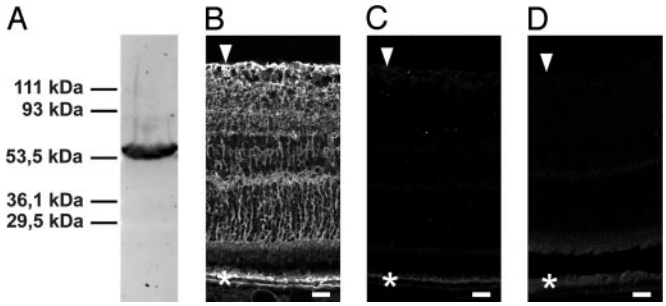

Fig. 1. Selectivity of antibody to CA XIV. (*A*) Immunoblot of membrane fraction of mouse retina reveals a single band at ≈54 kDa. (*B*) Immunofluorescence of CA XIV in mouse retina. (*C* and *D*) No specific labeling remains after preabsorption of the primary antibody with the immunizing recombinant CA XIV (*C*) or after omission of the primary antibody (*D*). Weak autofluorescence occurs in the RPE (*C* and *D*). Arrowheads indicate inner limiting membrane, and asterisks indicate RPE. (Scale bars: 20 μm.)

Antibody. We used total IgG isolated by protein A Sepharose chromatography from antisera raised in rabbits against a secretory form of mouse CA XIV (21). See *Supporting Materials and Methods*, which is published as supporting information on the PNAS web site, for details of this procedure. Immunoreactivity against retina was preabsorbed by the recombinant secretory form of CA XIV, confirming the selectivity of the antibody (11). A similar rabbit antibody raised to the secretory form of CA XIV was validated independently by showing lack of immunoreactivity in retina of the CA XIV knockout mice (15).

Western Blot. After homogenization and solubilization, extracts of mouse retinae (25 μl of supernatant, about half of a retina per lane) were loaded onto a 10% SDS/PAGE gel and subsequently transferred onto 0.2-μm poly(vinylidene difluoride) membrane (Bio-Rad). The membrane was probed with anti-mouse CA XIV diluted 1:6,000, developed by using alkaline phosphatase substrate (ECF Western blotting reagents, Amersham Pharmacia Biosciences), and visualized with a Typhoon Variable Mode Imager (Amersham Pharmacia Biosciences).

Immunocytochemistry. Animals were deeply anesthetized by an i.p. injection of a mixture of chloral hydrate, magnesium sulfate, and pentobarbital (170, 84, and 38.8 mg/kg of body weight, respectively). Retinae were fixed by transcardiac perfusion (12.5 ml/min, 15 min) with either phosphate-buffered 4% formaldehyde, pH 7.4, or bicarbonate-buffered 4% formaldehyde, pH 6.0, followed by 4% formaldehyde, pH 10.5 (pH shift protocol; 0.2% picric acid was added to both solutions).

Light microscopic immunocytochemistry was performed by using a method of indirect immunofluorescence (22). The antibody was diluted 1:100 or 1:200. Retinal sections were viewed and photographed with a Zeiss LSM 5 Pascal confocal microscope. Controls included preincubation of anti-CA XIV (1:200) with excess immunizing recombinant CA XIV (10 μg/ml) or omitting the anti-CA XIV antibody in the primary incubation solution.

For electron microscopic immunocytochemistry, small blocks of the eyecup were subjected to freeze substitution and infiltrated in Lowicryl as described (23). Ultrathin sections were processed for immunogold cytochemistry (24) with the CA XIV antibody (1:200) followed by gold-conjugated secondary antibody (15-nm particles).

Quantification and Statistical Analysis. Digital images were acquired with a commercially available image analysis program

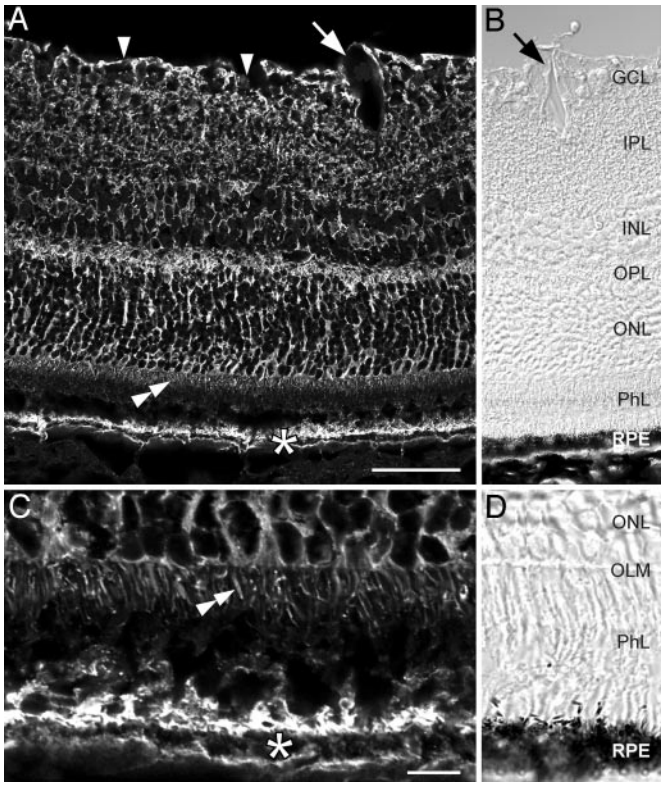

Fig. 2. Distribution of CA XIV immunoreactivity in the retina. The same antibody as in Fig. 1 is shown. (*A*) Immunolabeling extends throughout the neural retina and RPE (*). Note the dense labeling of RPE, outer plexiform layer, and inner limiting membrane (arrowheads). The immunofluorescent signal is particularly intense at the apical membrane of the RPE and is also quite pronounced at the inner aspect of the subretinal space [corresponding to the microvilli of the Müller cells (double arrowhead)]. Arrow indicates large vessel. (*B*) Interference optics, the same section as in *A* (arrows in *A* and *B* denote the same vessel). GCL, ganglion cell layer; IPL, inner plexiform layer; INL, inner nuclear layer; OPL, outer plexiform layer; ONL, outer nuclear layer; PhL, photoreceptor layer. (*C*) CA XIV immunolabeling in the outer retina. Note tiny immunopositive processes (double arrowhead) delimiting the inner aspect of the subretinal space. No labeling is seen over photoreceptor outer segments in PhL. The RPE (*) is intensely labeled apically and moderately labeled basally. (*D*) Interference optics, the same section as in *C*. OLM, outer limiting membrane. (Scale bars: *A*, 50 μm; *C*, 10 μm.)

(ANALYSIS, Soft Imaging Systems, Münster, Germany). Images of membrane segments were recorded at a nominal magnification of 34,500 × in 1,280 × 1,024 (16-bit) images. Each image represented a 2.72 × 2.17-μm rectangle, and each pixel represented a 2.1 × 2.1-nm square at the level of the specimen.

To avoid the effect of inadvertent differences in general labeling intensity, statistical comparisons were made between membrane domains sampled from one section (section code 11299A1; 386 images). Membrane segments of interest were drawn in the overlay and assigned a type label. Gold particles in the neighborhood of each membrane curve were detected semiautomatically, and the distance between the center of gravity of each particle and its membrane curve was calculated by the program. All images, with associated curves, particles, and measurements, were saved to allow later verification and correction.

Further analyses were done partly in ANALYSIS and partly in SPSS. The means of particle densities were compared between the groups, using the SPSS ANOVA with Scheffé's post hoc test.

For additional details of methods, see *Supporting Materials and Methods*.

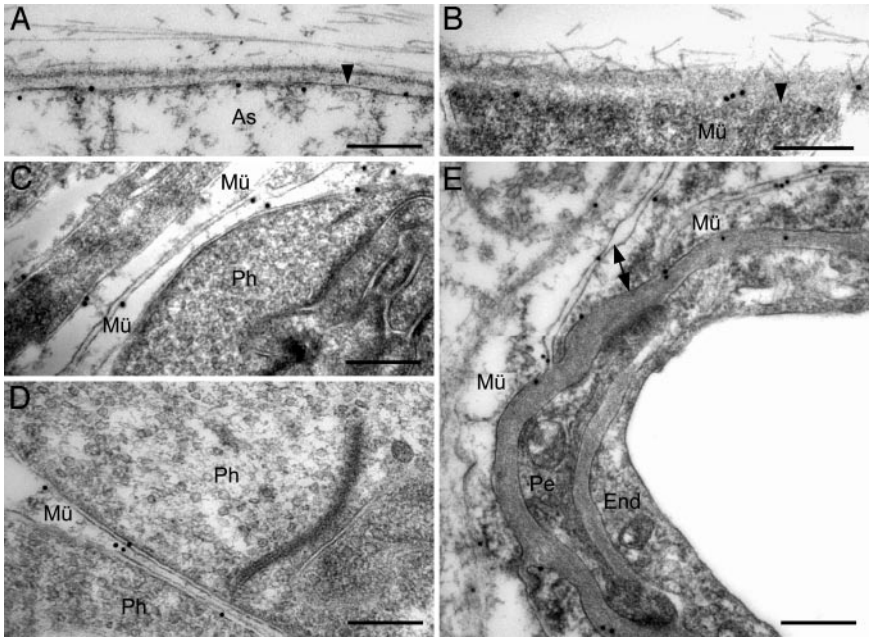

Fig. 3. Electron micrographs showing CA XIV immunoreactivity in the retina. (*A* and *B*) Gold particles signaling CA XIV are associated with subvitreal endfeet membranes of astrocytes (As) and Müller cells (Mü). Arrowheads indicate vitreal surface. (*C* and *D*) CA XIV immunopositive Müller processes in the outer plexiform layer are sandwiched between immunonegative photoreceptor terminals (Ph). (*E*) CA XIV is expressed in perivascular endfeet of Müller cells, with a stronger labeling in the membrane facing the vessel than in the membrane facing the neuropil. Double arrow spans the distance between the two membrane domains. Endothelial cells (End) and pericytes (Pe) are immunonegative. (Scale bars: 0.25 μm.)

Results

Western Blot and Immunofluorescence. Western blot analysis of mouse retina revealed a single band at ≈54 kDa, after incubation with the CA XIV antibody (Fig. 1*A*). A corresponding band was recorded in blots of brain extracts (data not shown), in agreement with Parkkila *et al.* (11). The antibody produced immunostaining spanning the entire radial extent of the retina (Fig. 1*B*). The labeling of the neural retina was abolished by preabsorption with the immunizing recombinant enzyme (Fig. 1*C*) or by omitting the primary antibody (Fig. 1*D*). Weak autofluorescence remained in the RPE.

Analysis at higher magnification showed labeling of delicate processes in all layers of the neural retina except in the outer part of the photoreceptor layer (Fig. 2*A*). The immunofluorescent processes were particularly concentrated in the outer plexiform layer, in the inner limiting membrane, and around blood vessels. A laminar pattern of labeling was apparent in the inner plexiform layer. Peripheral to the outer limiting membrane the labeling was concentrated in slender processes (Fig. 2*C*) that were identified as Müller cell microvilli at the EM level (see Fig. 4 *A* and *B*). The strongest immunofluorescent signal was recorded in the RPE. Labeling was particularly dense at the apical surface, corresponding to the microvilli, but was also quite distinct at the basal surface (Fig. 2*C*).

Immunogold Electron Microscopy. The postembedding immunogold analysis confirmed and extended the immunofluorescence data. Strong membrane-associated labeling occurred at astrocyte and Müller cell endfeet facing the corpus vitreum and blood vessels (Fig. 3 *A*, *B*, and *E*). Gold particles also decorated the thin Müller cell processes that are sandwiched between the neuronal elements of the outer plexiform layer (Fig. 3 *C* and *D*). Endothelial cells and pericytes displayed only scattered particles, not above background labeling (see Figs. 5 and 6).

A more detailed analysis of the outer retina showed strong immunolabeling of microvilli at either side of the subretinal space, i.e., in Müller cells and RPE, respectively (Fig. 4). The linear particle density was higher in the RPE microvilli than in the Müller cell microvilli (confirmed by quantitative analysis) (Fig. 5; see also Fig. 7, which is published as supporting information on the PNAS web site). Only background level of labeling was recorded over photoreceptor membranes and in the interior of the RPE (Fig. 6).

CA XIV is predicted to be anchored to the cell surface by a membrane-spanning domain with the entire CA domain facing the exterior (21). The immunofluorescence and immunogold images showed labeling to be preferentially associated with the plasma membrane (Fig. 6*A*). A distinct peak, corresponding to the plasma membrane, was verified by recording the distribution of gold particles along an axis perpendicular to the cell surface. The labeling was found only on membranes of astrocytes and Müller cells and on apical and basal membranes of RPE. No peak was observed corresponding to neuronal plasma membranes (Fig. 6*B*, quantified for photoreceptors only).

The distribution curve across Müller cell plasma membranes showed that the gold particle density dropped to background level within 25 nm of the outer and inner aspects of the plasma membrane (Fig. 6). The background level of labeling was slightly lower external to the plasma membrane (corresponding to the perivascular basal lamina) than on the cytoplasmic side. The weak intracellular signal likely reflects newly synthesized CA XIV along the secretory pathway.

Based on the data in Fig. 6*A*, all particles within 23.5 nm of the plasma membrane were defined as membrane-associated and considered to signal epitopes attached to or integrated in the plasma membrane (cf. ref. 24). With this criterion the linear labeling density of distinct plasma membrane domains varied by a factor of >30, from 0.2 gold particles per μm (the background level on endothelial cell membranes) to 6.8 gold particles per μm (the high expression on microvilli of RPE cells).

Discussion

Until recently, the identity of the membrane-associated CA in retina was controversial. Hageman *et al.* (17) initially reported

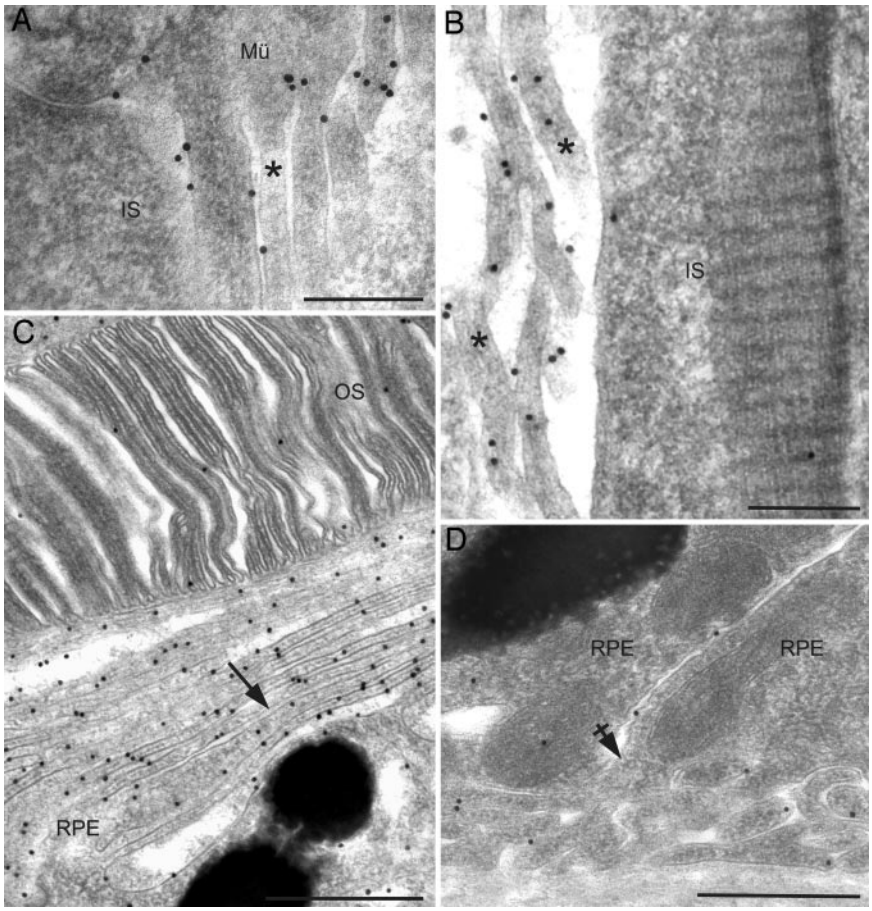

Fig. 4. CA XIV immunogold labeling in the outer retina. (*A* and *B*) Gold particles decorate microvilli (*) of Müller cells. Photoreceptor inner segments (IS) are immunonegative. (*C* and *D*) Microvilli (arrow in *C*) of RPE cells display stronger immunogold signals than the basolateral epithelial membrane (crossed arrow in *D*). Photoreceptor outer segments (OS) do not show immunogold labeling significantly above background level (compare Fig. 5*B*). Dark bodies represent pigment granules. (Scale bars: *A* and *B*, 0.25 μm; *C* and *D*, 0.5 μm.)

that there was no CA IV in retina although they demonstrated that it was highly expressed on the plasma face of the capillaries of the choriocapillaris. The issue became confused when Wolfensberger *et al.* (12) reported a 54-kDa protein in human retina, which they called CA IV. Because human CA IV is a 35-kDa nonglycosylated protein (25), it seems likely they misidentified CA XIV as CA IV, because the former had not yet been identified. From our own studies and those of Ochrietor *et al.* (15), it is clear that CA XIV is the major membrane-associated CA in retina. Neither CA IV nor CA XII, two other membrane CAs, are detectable in mouse retina on Western blots (15).

The present analysis addresses the subcellular distribution of CA XIV in retina. The two major findings are (*i*) a highly differentiated distribution of CA XIV along the Müller cell and astrocyte plasma membranes and (*ii*) an even more intense expression of CA XIV on the apical and, less so, basolateral surfaces of the RPE. In glial cells, CA XIV is present at low concentrations in membrane domains that abut neuropil and neuronal cell bodies, but is enriched in glial membrane domains that serve to delimit the neural retina facing other compartments (blood, corpus vitreum, and subretinal space). The three membranes in question (perivascular and subvitreal endfeet membranes and apical microvilli) express identical densities of CA XIV labeling, as judged from the quantitative analysis. However, given the enormous surface provided by the microvilli in RPE, the largest amount of CA XIV in the retina is found at the apical surface of the RPE.

Because CA XIV is expressed in astrocytes, Müller cells, and the RPE, its expression spans the entire thickness of the retina. This distribution pattern is consistent with involvement in extracellular pH regulation and its potential involvement in transretinal transport functions. Measurements of pH across the retinal layers have revealed that the pH increases on approaching the apical microvilli of the RPE (26). Studies with CA inhibitors suggest that an extracellular CA buffers the excess acidification in retina under certain metabolic conditions (such as under dark adaptation) by blunting the increase in H^+ concentration (27). Based on the strong expression of CA XIV on the basolateral membranes of RPE, one would predict a role for CA XIV in buffering the subretinal space volume as well.

Lactate is a by-product of high metabolic activity and must be cleared from active neuropil. The glial endfeet are likely to be involved in the export of excess lactate from retina to vitreous humor and blood. The enrichment of CA XIV at the endfeet may help maintain a favorable chemical gradient for lactate efflux, by consuming H^+ ions that are transported along with lactate through the endfeet membranes. In regard to this potential coupling of CA XIV activity and lactate transport, it is notable that the distribution pattern of the MCT1, which is believed to be responsible for a major fraction of lactate transport in the outer retina, is strikingly similar to that of CA XIV. Like CA XIV, MCT1 is strongly enriched in

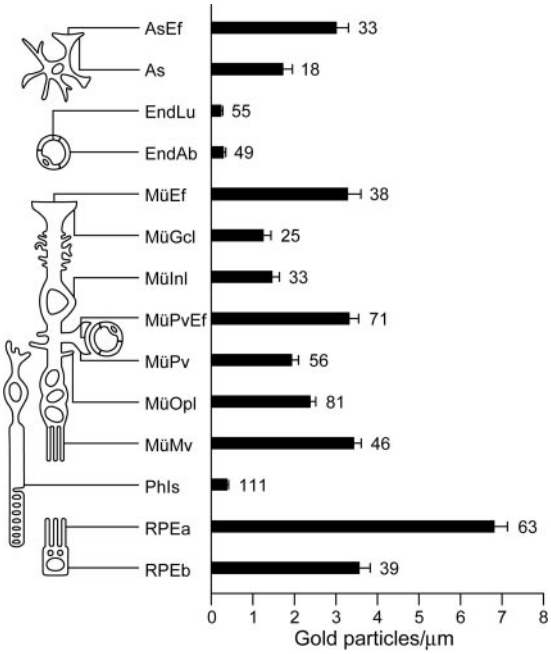

Fig. 5. Quantitative analysis of CA XIV immunogold labeling in specific membrane domains. Values along the abscissa represent the mean number of gold particles per micrometer of membrane, recorded at a primary magnification of ×34,500. Number of profiles and SEM are indicated. AsEf, membranes of astrocyte endfeet facing vitreal surface; As, lateral membranes of astrocyte endfeet; EndLu, luminal membranes of endothelial cells; EndAb, abluminal membranes of endothelial cells; MüEf, membranes of Müller cell endfeet facing vitreal surface; MüGcl, lateral membranes of Müller cell endfeet; MüInl, Müller cell membranes in the inner nuclear layer; MüPvEf, perivascular membranes of Müller cell endfeet; MüPv, lateral membranes of perivascular Müller cell endfeet; MüOpl, Müller cell membranes in the outer plexiform layer; MüMv, membranes of Müller cell microvilli; PhIs, membranes of photoreceptor inner segments; RPEa, apical membranes of RPE; RPEb, basolateral membranes of RPE. The statistical analysis of these data is presented in Fig. 7.

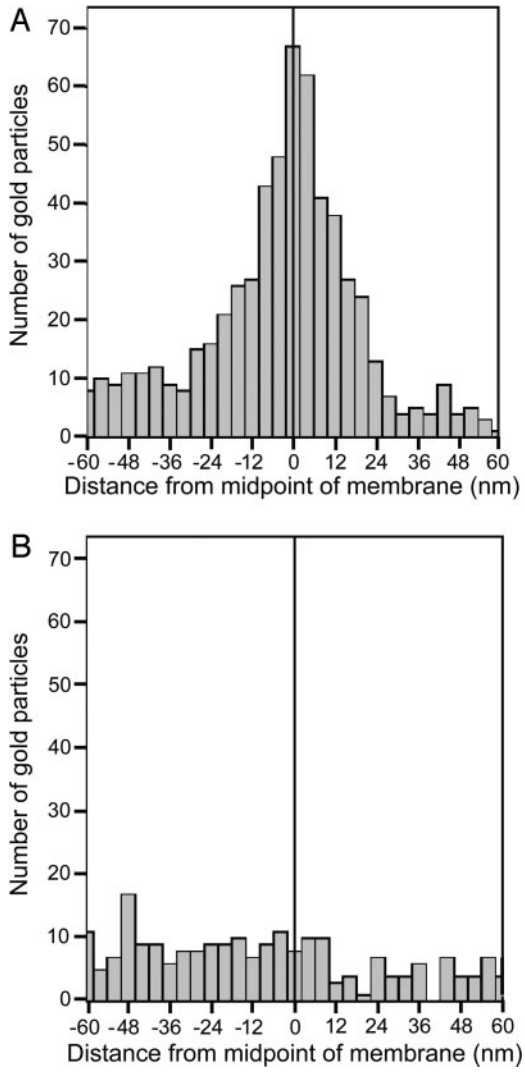

Fig. 6. Distribution of CA XIV signaling gold particles. Shown is particle distribution along an axis perpendicular to the perivascular plasma membrane of Müller cell endfeet (MüPvEf; *A*) and the plasma membrane of photoreceptor inner segments (PhIs; *B*) (compare Fig. 5). The ordinate indicates number of gold particles per bin (bin width, 4 nm; cytoplasmic side negative). The gold particle density drops to background level ≈25 nm from the midpoint of the plasma membrane [corresponding to the size of the antibody bridge between the epitope and the corresponding gold particle (24)]. The level of background labeling is slightly higher over cytoplasmic matrix (left in *A*) than over the perivascular basal lamina (right in *A*). There is no detectable peak over the photoreceptor plasma membrane (*B*).

the microvilli of the RPE and is also found in the microvilli of Müller cells (28). MCT1 is not significantly expressed in glial endfeet and basolateral membrane domains of RPE, but these membrane domains appear to contain MCT4 (unpublished observation) and MCT3, respectively (29).

The photoreceptors are one of the most metabolically active cell types in the body and generate large amounts of CO_2. The Müller cells are equipped to effect CO_2 removal as bicarbonate because they express both the electrogenic sodium-bicarbonate cotransporter, pNBC1 (30), and CA XIV in membrane domains facing photoreceptors. The enrichment of CA XIV in Müller cell endfeet might serve to direct CO_2 to the vitreous humor and retinal blood vessels. The clearance route for CO_2 and bicarbonate through RPE is likely to be extremely important also, given the high level of expression of CA XIV in RPE and the tight anatomic relationship between inner/outer segments of the photoreceptors and RPE apical processes.

The present finding of an enrichment of CA XIV in Müller cell endfeet is also of interest in regard to the pH sensitivity of retinal blood flow. An increased H^+ concentration in the perivascular space is known to cause vasodilation (31), implying that a high level of CA activity in endfeet might dampen activity-dependent increases in perfusion rate.

An important contrast in retina and brain is the presence of CA XIV on retinal glial cells and its absence on neurons. This is the opposite of the situation in brain where Parkkila *et al.* (11) found most of the staining on neuronal cell bodies and axons and none on glia. It is very interesting that retina, which is technically part of the CNS, should differ so fundamentally in this respect. This discrepancy likely reflects differences in the physiology of the two structures. Extracellular pH changes in retina that arise from light stimulation are quite different from the activity-dependent pH shifts in the brain, because the effect of light stimulation is to turn off the photoreceptor dark current and stop tonic synaptic transmission. The pH changes in retina result from the cessation of a high metabolic rate, i.e., from the absence of tonic activity (27). Ongoing synaptic activity in the dark causes continuous acidosis in retina. When this activity is turned off by light, a relative alkalosis occurs. In brain, however, activity causes a direct alkalosis. CA enzymatically suppresses the activity-induced alkaline pH shifts in the brain associated with excitation of pyramidal neurons (32, 33)

and enhances the alkaline pH shifts caused by activation of $GABA_A$ receptors (32, 34).

Finally, the finding of such intense CA XIV activity in RPE suggests that CA XIV is the retinal target of CA inhibitors, such as acetazolamide, when used to treat cystoid retinal edema. Prior publications by Wolfensberger and coworkers (12, 35–37) have suggested that inhibition of an RPE-associated, membrane-bound CA is sufficient to enhance subretinal fluid absorption and retinal adhesiveness in individuals with macular edema and other retinal conditions. Although this RPE-associated target for various CA inhibitors was assumed to be CA IV, the present study helps to resolve this issue by confirming that it is CA XIV, and not CA IV (15), that is associated with RPE and Müller cells.

We thank Dr. Paul Linser for sharing data before publication (15) and Professor Kai Kaila and four other expert reviewers for critical reading of the manuscript and helpful suggestions for revisions. This work was supported by the Nordic Centre of Excellence Program in Molecular Medicine and the Norwegian Research Council (Storforsk Program) (O.P.O.) and National Institutes of Health Grant DK40163 (to W.S.S.). A.C.B. is a Fulbright Fellow.

1. Chesler, M. (2003) *Physiol. Rev.* **83,** 1183–1221.
2. Wadiche, J. I., Amara, S. G. & Kavanaugh, M. P. (1995) *Neuron* **15,** 721–728.
3. Magleby, K. L. (2004) *Trends Neurosci.* **27,** 231–233.
4. Svichar, N. & Chesler, M. (2003) *Glia* **41,** 415–419.
5. McMurtrie, H. L., Cleary, H. J., Alvarez, B. V., Loiselle, F. B., Sterling, D., Morgan, P. E., Johnson, D. E. & Casey, J. R. (2004) *J. Enzyme Inhib. Med. Chem.* **19,** 231–236.
6. Pastorekova, S., Parkkila, S., Pastorek, J. & Supuran, C. T. (2004) *J. Enzyme Inhib. Med. Chem.* **19,** 199–229.
7. Agnati, L. F., Tinner, B., Staines, W. A., Vaananen, K. & Fuxe, K. (1995) *Brain Res.* **676,** 10–24.
8. Vardimon, L., Fox, L. E. & Moscona, A. A. (1986) *Proc. Natl. Acad. Sci. USA* **83,** 9060–9064.
9. Ghandour, M. S., Langley, O. K., Zhu, X. L., Waheed, A. & Sly, W. S. (1992) *Proc. Natl. Acad. Sci. USA* **89,** 6823–6827.
10. Ghandour, M. S., Parkkila, A. K., Parkkila, S., Waheed, A. & Sly, W. S. (2000) *J. Neurochem.* **75,** 2212–2220.
11. Parkkila, S., Parkkila, A. K., Rajaniemi, H., Shah, G. N., Grubb, J. H., Waheed, A. & Sly, W. S. (2001) *Proc. Natl. Acad. Sci. USA* **98,** 1918–1923.
12. Wolfensberger, T. J., Mahieu, I., Jarvis-Evans, J., Boulton, M., Carter, N. D., Nogradi, A., Hollande, E. & Bird, A. C. (1994) *Invest. Ophthalmol. Visual Sci.* **35,** 3401–3407.
13. Ruusuvuori, E., Li, H., Huttu, K., Palva, J. M., Smirnov, S., Rivera, C., Kaila, K. & Voipio, J. (2004) *J. Neurosci.* **24,** 2699–2707.
14. Linser, P. J., Ochrietor, J. D., Sly, W. S. & Grubb, J. H. (2001) *Invest. Ophthalmol. Visual Sci.* **42,** S772–S773.
15. Ochrietor, J. D., Clamp, M. F., Grubb, J. H., Shah, G. N., Waheed, A., Sly, W. S. & Linser, P. J. (2005) *Exp. Eye Res.*, in press.
16. Ridderstrale, Y., Wistrand, P. J. & Brechue, W. F. (1994) *Invest. Ophthalmol. Visual Sci.* **35,** 2577–2584.
17. Hageman, G. S., Zhu, X. L., Waheed, A. & Sly, W. S. (1991) *Proc. Natl. Acad. Sci. USA* **88,** 2716–2720.
18. Wang, L., Tornquist, P. & Bill, A. (1997) *Acta Physiol. Scand.* **160,** 75–81.
19. Newman, E. A. (1996) *J. Neurosci.* **16,** 159–168.
20. Newman, E. & Reichenbach, A. (1996) *Trends Neurosci.* **19,** 307–312.
21. Whittington, D. A., Grubb, J. H., Waheed, A., Shah, G. N., Sly, W. S. & Christianson, D. W. (2004) *J. Biol. Chem.* **279,** 7223–7228.
22. Veruki, M. L. & Wassle, H. (1996) *Eur. J. Neurosci.* **8,** 2286–2297.
23. Hjelle, O. P., Chaudhry, F. A. & Ottersen, O. P. (1994) *Eur. J. Neurosci.* **6,** 793–804.
24. Matsubara, A., Laake, J. H., Davanger, S., Usami, S. & Ottersen, O. P. (1996) *J. Neurosci.* **16,** 4457–4467.
25. Okuyama, T., Sato, S., Zhu, X. L., Waheed, A. & Sly, W. S. (1992) *Proc. Natl. Acad. Sci. USA* **89,** 1315–1319.
26. Yamamoto, F., Borgula, G. A. & Steinberg, R. H. (1992) *Exp. Eye Res.* **54,** 685–697.
27. Borgula, G. A., Karwoski, C. J. & Steinberg, R. H. (1989) *Vision Res.* **29,** 1069–1077.
28. Bergersen, L., Johannsson, E., Veruki, M. L., Nagelhus, E. A., Halestrap, A., Sejersted, O. M. & Ottersen, O. P. (1999) *Neuroscience* **90,** 319–331.
29. Philp, N. J., Yoon, H. & Grollman, E. F. (1998) *Am. J. Physiol.* **274,** R1824–R1828.
30. Bok, D., Schibler, M. J., Pushkin, A., Sassani, P., Abuladze, N., Naser, Z. & Kurtz, I. (2001) *Am. J. Physiol.* **281,** F920–F935.
31. Reber, F., Gersch, U. & Funk, R. W. (2003) *Graefes Arch. Clin. Exp. Ophthalmol.* **241,** 140–148.
32. Chen, J. C. & Chesler, M. (1992) *J. Neurophysiol.* **67,** 29–36.
33. Chen, J. C. & Chesler, M. (1992) *Proc. Natl. Acad. Sci. USA* **89,** 7786–7790.
34. Kaila, K., Paalasmaa, P., Taira, T. & Voipio, J. (1992) *NeuroReport* **3,** 105–108.
35. Wolfensberger, T. J., Dmitriev, A. V. & Govardovskii, V. I. (1999) *Doc. Ophthalmol.* **97,** 261–271.
36. Wolfensberger, T. J. (1999) *Doc. Ophthalmol.* **97,** 387–397.
37. Wolfensberger, T. J., Chiang, R. K., Takeuchi, A. & Marmor, M. F. (2000) *Graefes Arch. Clin. Exp. Ophthalmol.* **238,** 76–80.